ROOM TEMPERATURE TENSILE BEHAVIOR AND DAMAGE ACCUMULATION OF HI-NICALON REINFORCED SIC MATRIX COMPOSITES

G.N. Morscher*, Case Western Reserve University, Cleveland, OH

J.Z. Gyekenyesi*, Cleveland State University, Cleveland, OH

ABSTRACT

Composites consisting of woven Hi-Nicalon fibers, BN interphases, and different SiC matrices were studied in tension at room temperature. Composites with SiC matrices processed by CVI and melt infiltration were compared. Monotonic and load/unload/reload tensile hysteresis experiments were performed. A modal acoustic emission (AE) analyzer was used to monitor damage accumulation during the tensile test. Post test polishing of the tensile gage sections was performed to determine the extent of cracking. The occurrence and location of cracking could easily be determined using modal AE. The loss of modulus could also effectively be determined from the change in the velocity of sound across the sample. Finally, the stresses where cracks appear to intersect the load-bearing fibers correspond with high temperature low cycle fatigue run out stresses for these materials.

INTRODUCTION

The high temperature mechanical properties of SiC/SiC composites are limited due to oxidation reactions which occur in the presence of species such as oxygen and water vapor. What enables such reactions to occur at the fiber/interphase/matrix region of a composite is environmental ingress through pores in the matrix and/or through matrix cracks. For SiC/SiC composites where chemical vapor infiltration (CVI) is the matrix processing route, the fiber-matrix interphase region should be sealed off from the environment even though significant matrix porosity exists. Therefore, the environmental reactions are dependent on matrix cracking, although a highly porous matrix will allow the environment access to inner regions of a composite which would not be accessible if the matrix was dense. The composite fabrication method dictates the amount of porosity which exists in the matrix. The loading history of the composite, coupled with the flaw distribution in the matrix, dictate the amount and nature of cracking that exists in the matrix.

An understanding of the damage accumulation in a composite is critical in determining when matrix cracking occurs and the nature of matrix cracking, i.e. local microcracks or through-thickness cracks. Guillaumat and Lamon[1,2] have characterized

---

* Resident Research Associates at NASA Lewis Research Center; Cleveland, OH

the damage accumulation in a Nicalon™#, C interphase, CVI SiC matrix composite as a function of strain. They found that

1. Microcracks emanate from macropores between different fiber plies and propagate across the plies (ε = 0.025% to 0.12%)
2. Cracks then form and propagate in transverse (90°) bundles and dense matrix regions (ε = ~ 0.12% to 0.2%)
3. Finally, cracks form in the matrix surrounding 0° bundles ($\varepsilon \geq$ 0.2%)

The microcracks formed at large pores in the matrix and in 90° tows are sometimes referred to as tunnel cracks[3-5]. A slight reduction in elastic modulus would be expected from such cracking. When the microcracks intersect and debond the fiber/matrix interphases of the load-bearing fibers, significant elastic modulus reduction and unload/reload hysteresis behavior was observed[6].

This study will compare the stress-strain behavior of woven Hi-Nicalon™#, BN interphase, SiC matrix composites with melt infiltrated (MI) and CVI SiC matrices. Modal acoustic emission[7] will be used to monitor the damage accumulation and unload/reload hysteresis loops will be performed to determine the onset of damage in the 0° bundles as well as the interfacial properties of the two composite systems. The findings will then be related to the elevated temperature properties of these two composite systems.

EXPERIMENTAL

Table I: Woven Hi-Nicalon™, BN-interphase, SiC Matrix Composites

Composite	Composite Processing Details	Weave	V_f (loading direction)
CVI SiC	CVD BN interphase* CVI SiC matrix*	8 HS	0.15
MI SiC	CVD BN-interphase* 2 μm CVI SiC overcoat* Si melt infiltrated SiC matrix**	5 HS	0.17

- all composites were 0/90 lay ups with 8 plies (17 ends per inch)
* Dupont Lanxide: BN interphase; CVI SiC ** Carborundum: Melt Infiltration SiC
- specific processing details are proprietary

Table I describes the processing approaches, vendors, and woven architectures of the two composites compared in this study. The tensile sample dimensions and mounting arrangement are shown in Figure 1. The samples were cut from 152 mm x 229 mm plates into dogbone tensile specimens where the length was 203 mm, the width at the ends was 12.7 mm and the width at the gage section was ~10.2 mm. The plate thicknesses were nominally 2.35 and 2.2 mm for the CVI SiC and MI SiC composites, respectively. Tensile tests were performed with a screw-driven universal testing machine#. Glass fiber reinforced epoxy tabs (1.5 mm thick) were mounted on both sides of the

---

Nicalon™ and Hi-Nicalon™ produced by Nippon Carbon, Japan

Instron Model 8562, Instron Ltd., Canton, Mass.

sample in the grip regions. The specimens were gripped with rigidly mounted hydraulically actuated wedge grips. A clip on strain gage, with a range of 2.5% strain and 25.4 mm gage length was used to measure strain.

Wide-band (50 kHz to 2.0 MHz)[##], high fidelity sensors (9.2 mm in diameter) were placed just outside the tapered region of the dogbone sample to record acoustic emission events. Vacuum grease was used as a couplant and electrical tape was used to mount the sensors to the sample. Acoustic emission waveforms were recorded using a 2-channel, Fracture Wave Detector[##] (FWD). The FWD consisted of a personal computer (Pentium, 120 MHz) with a 12-bit, 30 MHz analog to digital acquisition board. Each sensor was connected to a preamplifier and filter trigger module which was fed into the computer. The preamplifier was set at 20 dB, the filter signal was amplified 3 dB, and the filter trigger was amplified 21 dB. The load and strain were also recorded with the FWD computer.

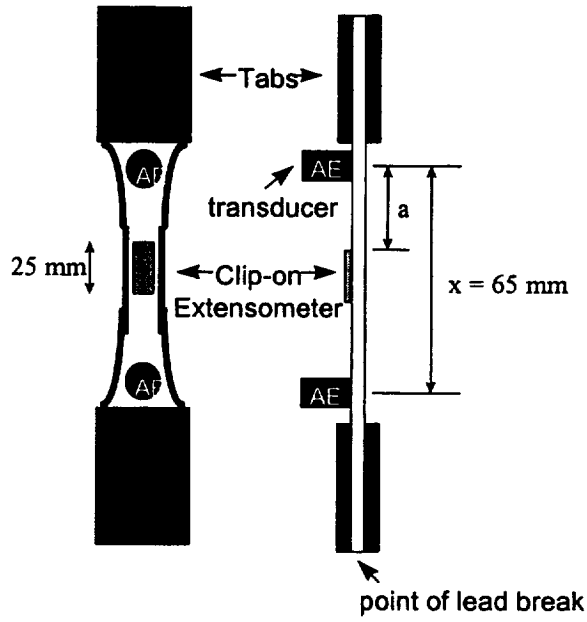

Figure 1: Specimen configuration.

The post-test analysis was performed on Wave Detector™ software provided by the FWD manufacturer.

RESULTS AND DISCUSSION

Typical monotonic tensile stress-strain curves are shown in Figure 2 for the two composites. The stress-strain behavior is very similar to that shown by other researchers for Nicalon/SiC woven composites[8-10]. Both composites failed at similar stresses (~ 380 MPa); however, the MI composites always failed in the grips whereas the CVI composites always failed in the gage section. The "knee" in the stress strain curve occurs at a lower stress for the CVI SiC composites and the strain to failure of the CVI SiC composites is greater than the strain to failure of the MI SiC composite. The mechanical properties of the two composites are listed in Table II.

Figures 3a and b show monotonic and hysteresis stress-strain curves of the two composite systems. The monotonic and hysteresis stress-strain curves are almost identical for both composite systems. The hysteresis stress-strain curves have slightly larger strains for the same stress compared to the monotonic stress-strain curves. For the hysteresis experiments, AE activity occurred in the gage section upon initial unloading and at the end of the subsequent reloading. This indicates a greater amount of damage in the hysteresis specimens[11] and could account for the increased strain incurred for hysteresis tensile tests.

[##] Digital Wave Corporation, Englewood, CO

The maximum loop width was determined for each unload/reload hysteresis loop at the stress which was half the maximum stress of the specific loop (Figure 4). The onset of 0° cracking is considered to occur when the hysteresis loop width is greater than zero. This occurs at ~ 110 MPa for CVI SiC composites and ~ 140 MPa for the MI SiC composites. It is also interesting to note that the loop width of the MI SiC composites were greater than that of the CVI SiC composites at higher stresses. It was observed from polished sections of failed composites that CVI SiC composites had almost three times the number of cracks of MI SiC (Table II).

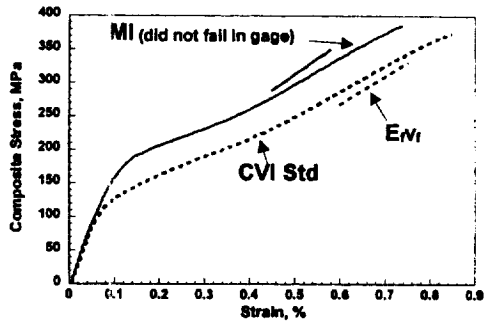

Figure 2: Monotonic stress-strain curves for MI SiC and CVI SiC composites.

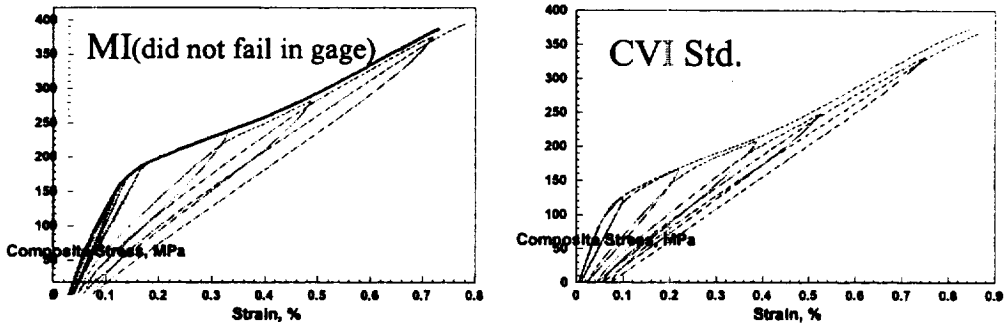

(a) (b)

Figure 3: Monotonic and unload/reload hysteresis tensile stress-strain curves for MI (a) and CVI (b) composites.

The modal AE analysis was used to discern the location of events which occurred in the gage section of the composites[11]. This is an important factor to determine because the number of events recorded for the monotonic experiments was ~ 7000 and 9000 for the MI and CVI SiC composites, respectively, whereas only ~ 1500 and 1250 events actually occurred in the gage section for the two composites, respectively. Modal AE analysis, as

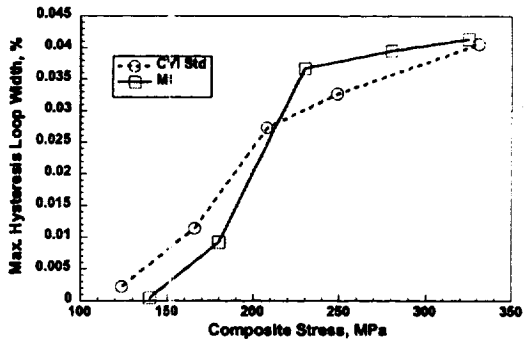

Figure 4: Hysteresis loop width for the two composites versus the peak stress of the hysteresis loop.

opposed to traditional AE* , involves the digitization of the real AE waveforms and analysis of the "modes", i.e. extensional (longitudinal) and flexural, of sound travel that make up the individual waveforms.

In order to determine the location of the events, the change in the speed of sound must be known for the stress-strain condition. This was done, as described in ref. 11, for the extensional wave from AE events which occurred outside of the two sensors during the tensile test. If the speed of sound is known as a function of strain, then, the elastic modulus as a function of strain can be determined. The speed of sound of the extensional wave, C_e, is related to elastic modulus, E_o, by:

$$C_e = [E_o / \rho (1-\nu^2)]^{1/2} \qquad (1)$$

where ρ is the density and ν is Poisson's ratio. The $E_o^{1/2}$ at a given strain can be normalized by $E_o^{1/2}$ at $\varepsilon = 0$ and C_e at a given strain can be normalized by C_e at $\varepsilon = 0$. The normalized $E_o^{1/2}$ and normalized $C_e^{1/2}$ should have the same relationship as shown in Figure 5 for the unload/reload hysteresis tensile tests where E_o was determined from the tangent modulus upon initial unloading of the hysteresis loop[6]. There is excellent agreement between the reduction in modulus and the reduction in the speed of sound for both composites. In fact the modulus and speed of sound decreases are the same relative to the initial modulus (Table II) and speed of sound of the undamaged material for both composites, respectively. This is not too surprising since both composites appear to have reached or nearly reached matrix crack saturation and both composites failed at similar stress levels which would result in a similar *overall* stress distribution on the fibers over the entire gage length (assuming a constant interfacial shear strength).

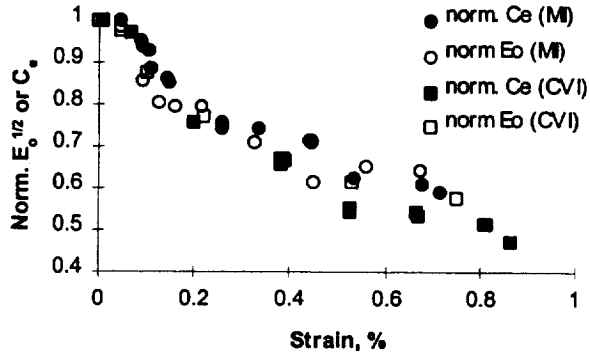

Figure 5: Normalized $E_o^{1/2}$, $\{E_o(\varepsilon)/E_o(\varepsilon=0)\}^{1/2}$, and normalized C_e, $C_e(\varepsilon)/C_e(\varepsilon=0)$, plotted versus composite strain for the two composites from unload/reload hysteresis tensile experiments.

The specific gage events were identified from (i) the difference in time of arrival between the two sensors (Figure 1) for a given event and (ii) the change in the speed of sound as the damage in the material increases[11]. Figure 6 shows the AE data for the two composites tested monotonically in tension to failure. The AE data show the same general trend for the two composites. Initially, rapid AE activity is occurring up to the "knee" in the stress strain curve. The rate of AE activity then decreases substantially. For the CVI SiC composite, an increase in the rate of AE activity occurred just prior to

* In traditional AE, the real sound wave is fit to a damped sine curve and AE parameters such as counts, amplitude, duration, energy, etc... are tabulated and saved. Resonant frequency transducers are used with traditional AE which cannot detect the wide frequency range of the real waveform that is produced by a fracture event. See references 7 and 11 for greater detail concerning the differences between the two types of AE analysis.

failure; whereas this did not happen for the MI material. The onset of AE activity in the gage section occurred at lower stresses and strains for the CVI composite (Table II). However, the total amount of AE events recorded was greater for the MI composite. It should also be noted that the "loudest" or highest energy events occur predominantly at the lower strains where the rate of AE activity was most rapid[11].

Table II: Results from Tensile Tests

Composite [# tests]	Ultimate Strength (MPa)	Elastic Modulus (GPa)	1st AE Noise Stress (MPa)	1st 0° Cracking Stress (MPa) [LCF stress]#	Avg. Crack Spacing (mm)	Avg. τ (MPa)
CVI Std. [2m, 2h]	370 ± 5	195 ± 5	55	~ 110 **[103]**	0.34	36 ± 8
MI* [4m, 2h]	>390±5	214 ± 6	74	~ 140 **[143]**	0.87	11 ± 3

Low Cycle Fatigue (2 hr hold, unload/reload cycle) run out stress (500 hours)
* did not fail in gage section

The tapering off of the AE activity is most likely due to the decrease in matrix cracking or matrix crack saturation (~ 0.35% strain). The inflection in the stress-strain curve is also indicative of matrix crack saturation. The occurrence of AE activity near the ultimate strength for the CVI material is probably due to the initiation of fiber failures in the gage section[11]. This did not happen for the MI material because it did not fail in the gage.

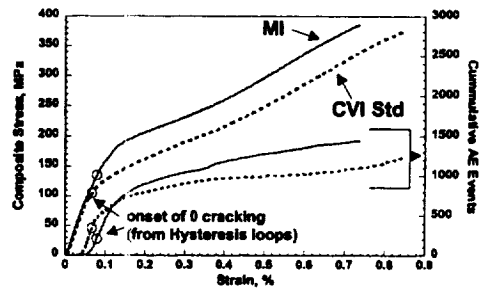

Figure 6: AE activity for monotonic stress strain curves of two composites.

Also noted on Figure 6 is the point on the stress-strain and AE event-strain curves where the onset of 0° cracking was determined (Figure 4). Note that ~ 350 AE events occurred prior to this stress in the CVI material and ~ 200 AE events occurred prior to this stress in the MI material. For the CVI material, the number of AE events occurring prior to the onset of 0° cracks accounts for over 25% of the total number of AE events occurring in the gage section. Evidently, a significant number of microcracks in the matrix and 90° bundles were formed in these materials prior to the extension or formation of cracks which significantly intersect the load-bearing fibers.

The gage sections of the failed composites were cut and polished longitudinally in the gage section to determine the amount and extent of cracking (Figures 7 and 8). For both systems, each crack could essentially be traced completely through the composite from one edge or side of the composite to the other. The cracks appeared to be transverse within a ply, but could deviate up or down between plies. The number of cracks were counted over the length of the gage sections and the average crack spacing was found to be 0.34 mm and 0.87 mm for the CVI and MI composites, respectively. In

other words, nearly three times as many cracks occurred in the gage section for the CVI composites compared to the MI composites.

The most striking difference between the two composites is the porosity of the CVI matrix composite. In the CVI composites, similar to refs. 1 and 2, cracking appeared to emanate primarily from the large, jagged regions (figure 7b) of the pores which existed between 90° tows and in-between plies or on the surface at the intersection of a 0 and 90° tow. For the MI composites, such pores and jagged regions did not exist and it was impossible to discern where the origin of the cracks occurred. Presumably they occurred at surface flaws, large matrix regions, and/or in the 90° bundles.

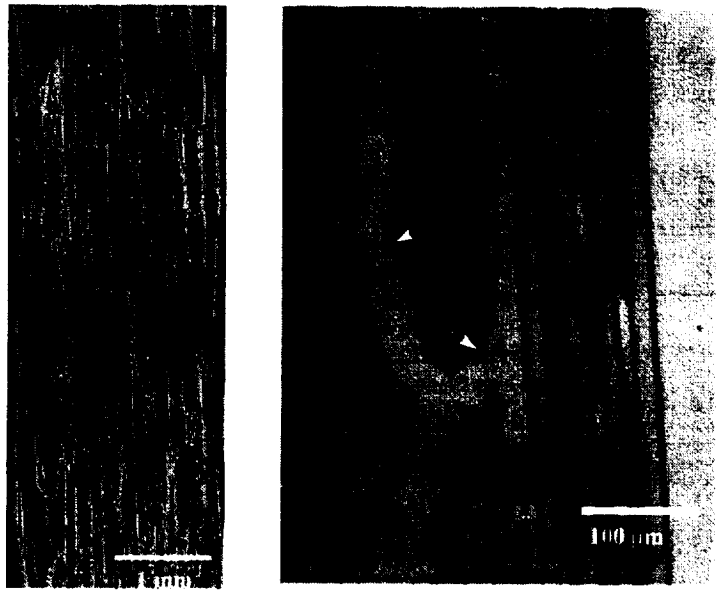

(a) (b)

Figure 7: Lower magnification (a) and higher magnification (b) optical micrographs of polished longitudinal section of CVI composite tested in tension to failure. Arrows indicate cracks.

The interfacial shear stress, τ, was determined from the hysteresis loop width, $\delta\varepsilon_{max}$, and average matrix crack spacing, d_c, for the composites from the relationship[6]:

$$\tau = (\sigma_p^2/2\delta\varepsilon_{max})\,[b_2(1-a_1v_f)^2(R_f/d_c)/\{4v_f^2E_m\}] \quad (2)$$

where, σ_p is the hysteresis loop peak stress, b_2 and a_1 are coefficients given by Hutchinson and Jensen[12], R_f is the average fiber diameter (13 microns), and E_m is the elastic modulus of the matrix (400 GPa). In order to approximate d_c for each hysteresis loop, the average crack spacing was assumed to be indirectly proportional to the AE activity (similar to Figure 6). For the σ_p of a given hysteresis loop, the final d_c measured after fracture was multiplied by the final number of AE events in the gage and divided by the number of AE events which occurred in the gage up to σ_p. The larger $\delta\varepsilon_{max}$ and d_c for the MI composites resulted in a τ value less than one third that of the CVI composites. This could be due to differing residual stress states from the different matrix processing routes used to fabricate the composites. However, it is most likely that the difference in τ was due to the formation of a carbon layer between the fibers and the BN interphase in the MI composites. The processing temperature for MI SiC is at least that of the melting temperature of Si (~ 1410°C). The Hi-Nicalon™ fibers undergo some decomposition above about 1400°C which results in the formation of a carbonaceous layer at the surface of the fiber[13]. Transmission electron microscopy studies on similar composites have shown that a thin carbon layer does exist between the fiber and the BN for Hi-

Nicalon™/BN/MI SiC composites and has not been observed for Hi-Nicalon™/BN/CVI SiC composites[14].

The nature of damage accumulation is expected to influence the elevated temperature life properties of CMC's. Some data exists[15-16] for low-cycle fatigue, LCF, tests performed on these same types of composites at 815°C in air. The LCF cycle consisted of a loading step to the peak stress, a 2 hour hold at the peak stress followed by an unloading step down to a minimum stress value. The run-out condition for these experiments was set at 250 cycles (500 hours at the peak stress). It was found that the run-out stresses for the CVI and MI composites were 103 MPa and 143 MPa respectively. These are nearly identical with the onset of 0° cracking as determined from the hysteresis tensile tests (Table II). Evidently, for this composite life criteria, the stress where the onset of cracking occurs was not life limiting. Instead, it was the stress where crack growth or crack formation resulted in the intersection of the load-bearing fibers. The LCF peak stress was about twice the stress at which cracking was first detected in the gage section of these composites. This of course assumes that the onset of cracking at 815°C is the same as at room temperature. Lipetzky et al[10] have shown that for a Nicalon-CVI SiC composite the modulus, proportional limit and damage regime slope of the tensile stress-strain curve up to 1200°C is essentially unchanged. Since these properties do not change it is reasonable to assume that the onset of cracking is essentially the same over this temperature range.

Figure 8: Lower magnification (a) and higher magnification (b) optical micrographs of polished longitudinal section of MI composite tested in tension to failure. Arrows indicate cracks.

CONCLUSION

The mechanical properties and damage accumulation of Hi-Nicalon, BN interphase woven composites with CVI SiC and MI SiC matrices were determined and compared. The ultimate and elastic properties of the two composites were similar; however, the onset of cracking occurred at lower stresses and strains for the CVI composite system. This was due to the large, jagged pores which exist in the CVI SiC matrix and were the site of initial cracking for these composites. MI SiC matrix composites did not have such pores. Modal acoustic emission was found to be a useful technique to monitor the onset and continuum of damage which occurred *in the gage section* of the tensile specimens tested. The decrease in the speed of sound as increasing damage occurred with increasing stress could be used to determine the elastic modulus with increasing damage accumulation.

Fewer cracks occurred in the gage section for MI composites due to the lower interfacial shear strength of these composites. It was presumed that the lower interfacial strength of the MI composites was due to the formation of a carbon layer at the fiber matrix interphase due to the decomposition of the fibers during processing.

Finally, the stresses for both composite systems where cracks intersected the load-bearing bundles (0° cracking) could be correlated to the life-limiting stresses from

elevated temperature low cycle fatigue tests performed in air at 815°C; even though cracking had occurred in the composites at stresses which were half the stress for 0° cracking.

ACKNOWLEDGEMENT

This work was supported by the HITEMP program at NASA Lewis Research Center, Cleveland, OH.

REFERENCES

1. L. Guillaumat and J. Lamon, "Multi-fissuration de Composites SiC/SiC," in Revue des Composites et des Materiaux Avances, vol. 3, pp. 159-171 (1993)
2. L. Guillaumat and J. Lamon, "Probabilistic-Statistical Simulation of the Non-Linear Mechanical Behavior of a Woven SiC/SiC Composite," Comp. Sci. Tech., **56,** 803-808 (1996)
3. D.S. Beyerle, S.M. Spearing, and A.G. Evans, "Damage Mechanisms and the Mechanical Properties of a Laminated 0/90 Ceramic/Matrix Composite," J. Am. Ceram. Soc., **75**, 3321-30 (1992)
4. S. Ho and Z. Suo, "Tunneling Cracks in Constrained Layers," J. Appl. Mech., 60, 890-94 (1993)
5. Z.C. Xia, R.R. Carr, and J.W. Hutchinson, "Transverse Cracking in Fiber Reinforced Brittle Matrix, Cross-Ply Laminates," Acta Metall. Mater., 41 [8] 2365-76 (1993).
6. J.M. Domergue, F.E. Heredia, and A.G. Evans, "Hysteresis Loops and the Inelastic Deformation of 0/90 Ceramic Matrix Composites," J. Am. Ceram. Soc., 79 [1] 161-70 (1996)
7. M. R. Gorman, "New Technology for Wave Based Acoustic Emission and Acousto-Ultrasonics," AMD-Vol. 188, Wave Propagation and Emerging Technologies, ASME, pp. 47-59 (1994)
8. M. Leparoux, L. Vandenbulcke, S. Goujard, C. Robin-Brosse, and J.M. Domergue, "Mechanical Behavior of 2D-SiC/BN/SiC Processed by ICVI," Proc. ICCM-10, Vol. IV, 633-640 (1995).
9. C. Droillard and J. Lamon, "Fracture Toughness of 2-D Woven SiC/SiC CVI-Composites with Multilayered Interphases," J. Am. Ceram. Soc., 79[4] 849-58 (1996)
10. P. Lipetzky, G.J. Dvorak, N.S. Stoloff, "Tensile Properties of a SiCf/SiC Composite," Mater. Sci. Eng. A216 pp. 11-19 (1996).
11. G.N. Morscher, "Modal Acoustic Emission of Damage Accumulation in a Woven SiC/SiC Composite," submitted to Comp. Sci. Tech.
12. J.W. Hutchinson and H. Jensen, "Models of Fiber Debonding and Pull-Out in Brittle Composites with Friction," Mech. Mater., 9, 139-63 (1990)
13. G. Chollon, R. Pailler, R. Naislain, F. Laanani, M. Monthioux, and P. Olry, "Thermal Stability of a PCS-derived SiC Fibre with a Low Oxygen Content (Hi-Nicalon)," J. Mater. Sci., 32, 327-47 (1997)
14. J. Brennan, unpublished research.
15. D. Brewer, NASA Lewis Research Center, unpublished research.
16. G.N. Morscher, "Embrittlement of Hi-Nicalon™, BN, CVI and MI SiC Matrix Composites in Air at Elevated Temperatures, " to be presented at the 1998 Annual American Ceramic Society Meeting.